

# Vacancy defects and defect clusters in alkali metal ion-doped MgO nanocrystallites studied by positron annihilation and photoluminescence spectroscopy

S. Sellaiyan<sup>1</sup> · A. Uedono<sup>1</sup> · K. Sivaji<sup>2</sup> · S. Janet Priscilla<sup>2</sup> · J. Sivasankari<sup>3</sup> · T. Selvalakshmi<sup>4</sup>

Received: 20 April 2016 / Accepted: 15 September 2016 / Published online: 27 September 2016  
© Springer-Verlag Berlin Heidelberg 2016

**Abstract** Pure and alkali metal ion (Li, Na, and K)-doped MgO nanocrystallites synthesized by solution combustion technique have been studied by positron lifetime and Doppler broadening spectroscopy methods. Positron lifetime analysis exhibits four characteristic lifetime components for all the samples. Doping reduces the Mg vacancy after annealing to 800 °C. It was observed that Li ion migrates to the vacancy site to recover Mg vacancy-type defects, reducing cluster vacancies and micropores. For Na- and K-doped MgO, the aforementioned defects are reduced and immobile at 800 °C. Coincidence Doppler broadening studies show the positron trapping sites as vacancy clusters. The decrease in the  $S$  parameter is due to the particle growth and reduction in the defect concentration at 800 °C. Photoluminescence study shows an emission peak at 445 nm and 498 nm, associated with  $F_2^{2+}$  and recombination of higher-order vacancy complexes. Further, annealing process is likely to dissociate  $F_2^{2+}$  to  $F^+$  and this  $F^+$  is converted into F centers at 416 nm.

## 1 Introduction

Magnesium oxide (MgO), a distinctive wide band gap (7.2 eV) insulator, is widely used in many applications across multiple domains [1–5]. Nevertheless, it has high melting point and easy to prepare due to the high oxygen affinity and low melting temperature of Mg. Hence, many researches have carried out the synthesis and characterization of nano-MgO as powder form owing to the interesting characteristics [6–10]. The nature of defect present in oxide materials such as MgO,  $TiO_2$ , and ZnO has found tremendous application in optoelectronic devices [11]. They play an important role in both the chemical and physical behaviors of oxide materials. Point defects have a profound effect upon the optical properties of solids [12]. It may be related to either oxygen vacancies or cation vacancies such as  $V_{Mg}$  in MgO, which are distributed on the surface of nanoparticles [13]. Mageshwari et al. [14] reported that the variation in concentration of defects is strongly related to the synthesis condition, surface morphology, and crystallite size. Furthermore, surface functionalization of nanocrystalline oxide materials can lead to unexpected optical properties [15] and makes them a promising candidate for inorganic phosphors [16]. In MgO nanocrystallites, the presence of defects was due to the bond breaking and surface stress caused by large surface-to-volume ratio [17]. The optical absorption measurements and many-body theory calculations of MgO predict that the  $F^+$  center is an easier way to identify charge state of the oxygen vacancy and offer a reinterpretation of the assignments of emission peaks to different charge states of the F center in MgO [18]. Pikhitsa et al. [19] determine that a defect, responsible for emission bands, creates proximal anion–cation vacancy pairs named P centers that may appear instead of F centers because of changes in the MgO

✉ S. Sellaiyan  
selva2d@gmail.com

<sup>1</sup> Division of Applied Physics, University of Tsukuba, Tsukuba, Ibaraki 305-8573, Japan

<sup>2</sup> Department of Nuclear Physics, University of Madras, Chennai 600025, India

<sup>3</sup> Department of Physics, Anna University, MIT Campus, Chennai 600044, India

<sup>4</sup> Nanomaterials Laboratory, Department of Physics, National Institute of Technology, Tiruchirappalli 620015, India

nanoparticle growth conditions. Xu et al. [20] studied the significant number of vacancy clusters located on the surface of gold nanoparticles embedded in MgO. Alkaline metals can be easily doped in alkaline-earth oxides, and this doping has been found quite useful in industry [21, 22]. When the Mg ion ( $\text{Mg}^{2+}$ ) of MgO lattice is substituted by alkali metals ( $\text{Li}^+$ ,  $\text{Na}^+$ ,  $\text{K}^+$ ), oxygen vacancy will be inevitably produced to maintain an overall neutral charge in MgO matrix. Lithium-doped MgO has promoted the generation of oxygen vacancy, whereas titanium-doped MgO hinders the generation of oxygen vacancy [23]. However, strong experimental evidence of the correlation between vacancy defects studied by positron annihilation and photoluminescence is still limited.

Positron annihilation lifetime spectroscopy (PALS) and Doppler broadening (DB) are nondestructive techniques to study vacancies and voids in solids [24]. Due to attractive potential in the negative and neutral charged defects, vacancy-type defects are effective positron trapping centers. The positron annihilation characteristics such as the positron lifetime and the electron momentum derived from the annihilation energy spectra from Doppler broadening of annihilation radiation are modulated by vacancy defects due to the reduced electron density and the change in electron momentum distribution. In porous materials, positronium (Ps), the bound state of positron–electron pair, may form in open spaces by exhibiting *para*-Ps (*p*-Ps), which is a singlet state, and *ortho*-Ps (*o*-Ps), which is a triplet state. *Ortho*-Ps primarily exhibits three-photon ( $3\gamma$ ) annihilation that produces a continuous energy distribution from 0 to 511 keV which provide information of microstructure of the pores.

The present study is aimed to find the role of alkali metal ions ( $\text{Li}^+$ ,  $\text{Na}^+$ , and  $\text{K}^+$ ) in MgO nanocrystallites and to find the type of vacancies, micropores in as-prepared and doped MgO nanocrystallites by PALS and coincidence Doppler broadening spectroscopy. We have also studied the reduction in vacancy defects in the nanocrystals during high-temperature annealing at 800 °C by aforementioned positron annihilation measurements. Variations in the photoluminescence behavior of all the samples were also studied to examine the role of defects in concentrations.

## 2 Experimental

Pure MgO-, Li-, Na-, and K-doped MgO have been synthesized by solution combustion method. The XRD patterns for the as-prepared and annealed samples have been reported by the authors [25]. The average crystallite size, as calculated from the Scherrer formula, is tabulated in Table 1. The synthesized powders were annealed at 500 °C (as-prepared) for 5 h in order to remove the residual

nitrate and further post-annealed to 800 °C for 1 h. Post-annealing further promotes the aggregation of Li, Na, or K centers and the crystallization of  $\text{XO}_2$  ( $\text{X} = \text{Li}, \text{Na}, \text{K}$ ) oxide clusters.

The positron lifetime spectra were measured using a digital lifetime spectrometer with digital storage oscilloscope (LeCroy Wavepro). In the  $\beta^+$  decay process of  $^{22}\text{Na}$ , a positron, the antiparticle of an electron, is released from the unstable isotope, along with a 1.28 MeV gamma ray signifying the birth of positron. In this process, positrons injected into the solid, gets thermalized, diffused and thereby losing its kinetic energy, which leads to annihilation with one of the free electrons ( $e^-$ ), resulting to the emission of two 511-keV annihilation photons. The annihilated photons (positron annihilation signals) are detected by two  $\text{BaF}_2$  scintillators coupled to H3378 (Hamamatsu Photonics) photomultiplier tubes (PMT). The PMT anode is separated into two: one connected to a constant fraction discriminator (CFD) and the other to a digital storage oscilloscope (DSO). The energy 1.28 MeV and annihilated photon energy 511 keV (positron birth and annihilated photons) signals from the CFDs are connected to the input of the coincidence unit. The output pulses are digitized and stored in the histogram memories in the DSO upon triggered by a 511-keV coincidence signal from the coincidence unit. All the measurements were taken to have count of statistics of  $6 \times 10^6$  counts. The measured lifetime spectra were analyzed, deconvoluted, and fitted with multiple exponential components in order to determine a number of lifetime components. The observed spectra were further analyzed with a experimental time resolution of 170 ps using the RESOLUTION computer program [26].

Coincidence Doppler broadening spectra were measured by using conventional spectrometer with two high-purity Ge detectors. When a positron is implanted into condensed matter, it annihilates with an electron and emits two 511-keV  $\gamma$  quanta. The energy distribution of the annihilation  $\gamma$  rays is broadened by the momentum component  $p_L$  of the annihilating electron–positron, which is parallel to the emitting direction of the  $\gamma$  rays. The energy of the  $\gamma$  rays is given by  $E_\gamma = 511 \pm \Delta E_\gamma$  keV. Here, the Doppler shift  $\Delta E_\gamma$  is given by  $\Delta E_\gamma = p_L c/2$ , where  $c$  is the speed of light. A freely diffusing positron may be localized in a vacancy-type defect due to positron affinity with an electron. The electron momentum distribution arises from such defects differs from that of in the bulk, and hence, these defects can be quantified from the Doppler broadening spectra arising from the annihilation radiation. This experimental technique is explained in detail elsewhere at the photo peak of 511 keV with energy resolution of  $\sim 1.2$  keV [27] with the channel width of 0.076 keV. For each of the measurements, a total of 10 million counts in

the annihilation peak were collected and then characterized from the shape parameters, i.e., the  $S$  and  $W$  parameters (with the  $W$  value calculated from the tail of the peak) in the range of  $4.56 \text{ keV} \leq |\Delta E_\gamma| \leq 6.84 \text{ keV}$ . The  $S$  denotes the annihilation from the valence electrons and the  $W$  denotes the annihilation from the core electrons extracted from the central and wing regions, respectively. In the present study, the positron lifetime and Doppler broadening spectra were measured simultaneously for the same sample set with independent experimental setups. The photoluminescence (PL) measurements were taken using JASCO FP8500, and samples were excited by employing 370 nm wavelength from Xe-lamp source. All the measurements were taken at 300 K.

### 3 Results and discussion

#### 3.1 Positron lifetime studies

Figure 1 shows the positron lifetime spectra and the corresponding intensity variation for MgO, MgO:Li, MgO:Na, and MgO:K for the as-prepared (at 500 °C) and annealed (at 800 °C) nanocrystallites. The analysis of the positron lifetime spectra for as-prepared samples revealed four lifetime ( $\tau$ ) components ascribed to two short lifetimes  $\tau_1$  and  $\tau_2$ , and long lifetimes  $\tau_3$  and  $\tau_4$ . The first lifetime,  $\tau_1$ , corresponds to the average lifetime of free positrons and trapped positrons at point defects and  $\tau_2$  corresponds to the annihilation lifetime due to positrons trapped in vacancy clusters. The two long lifetime components  $\tau_3$  and  $\tau_4$  originate from pick-off annihilation of *ortho*-positronium. The variation in fit was very high when we tried to fit as a single *ortho*-positronium component with background fitting and source component subtraction. Hence, these components are separated here, because the lifetime of those components shows large difference even their intensities of these two components are of the order of a few percent.

The undoped MgO which exhibited the shortest lifetime of 211 ps ( $\tau_1$ ) with intensity of 47 % ( $I_1$ ) is much higher to the earlier reported 166 ps [28]. The observed first lifetime is due to averaged lifetime of free positrons and some trapped positrons at Mg vacancy-type defects [29] and that could be a cause for higher lifetime (211 ps) when compared to earlier reported value.

The positron short lifetime of monovalent impurity such as Li, Na, and K on MgO is 171, 199, and 203 ps, respectively. These results indicate that the first-group elements occupied in Mg vacancy site such as point defects and extended defects. But the intensity ( $I_1$ ) of Li is only increased to 55 % rather than Na and K. So, the intensity reduction in first component is due to increase in  $I_2$

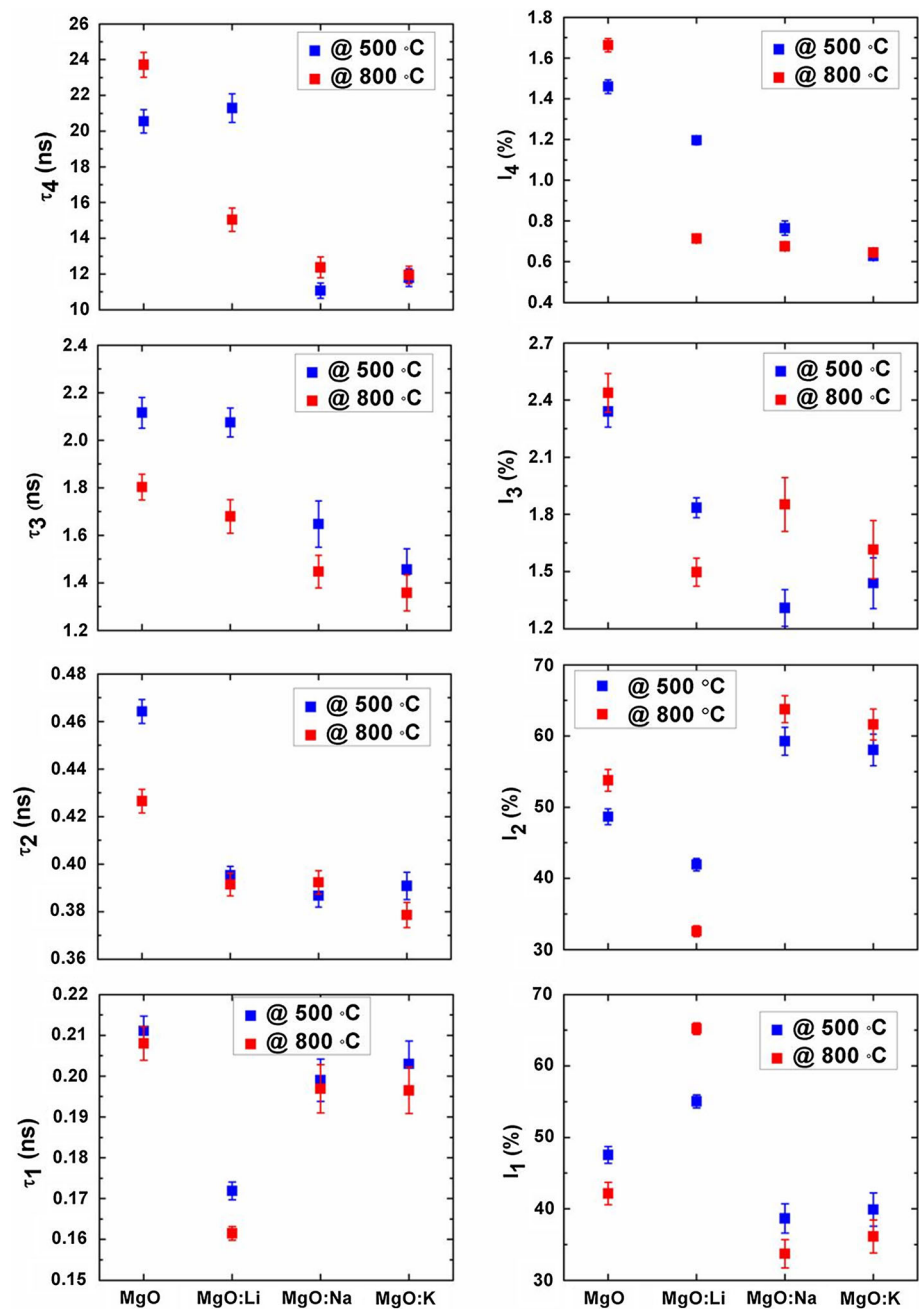
component of Na- and K-doped MgO which is discussed later. As Mg and Li ionic radii are almost same, Li has easily occupied by the vacancy rather than Na and K.

The second lifetime component ( $\tau_2$ ) is attributed to the positron trapped at the cluster vacancy defects in the crystallites and grain boundary [30], and the corresponding intensity from the as-prepared MgO is 48 % ( $I_2$ ) which gets reduced to 42 % after Li doping. This is due to the size of the cluster vacancy reduced with their intensity and easily occupied by the cluster vacancy in the grain boundary and the crystallites. On contrary, the intensity  $I_2$  is increased with Na and K doping, which might have precipitated in the grain boundary or occupied by small microvoids. These microvoids reduce as cluster vacancy and thus increasing the second lifetime component intensity of 59 and 58 % for Na and K, respectively. The average diffusion length of positrons is limited approximately to 50 nm which makes a number of positrons to reach grain boundary and trapped at the grain boundaries (the grain size is less than 50 nm range in the present studies). Hence, these vacancies and vacancy clusters are most probably located at the grain boundary region which is evident from  $\tau_1$  and  $\tau_2$  with related intensities.

The long lifetime components  $\tau_3$  and  $\tau_4$  due to *o*-Ps annihilation in small and large microvoids exist in MgO prepared by combustion method [31] and the lifetimes showed with reduced intensity. The size of the voids and their intensities of Na- and K-doped sample have been predominantly reduced due to most of the Na and K occupied in microvoids. However, Li occupied both the cluster vacancy as discussed above and the voids in MgO and thus small decrease in long lifetimes ( $\tau_3$  and  $\tau_4$ ) and their intensity. All as-prepared crystallite samples have defects such as vacancy-type defect, cluster vacancy, and microvoids. The lifetime of *o*-Ps can be greatly reduced by pick-off annihilation, with lifetime closely related to the size of the voids.  $\tau_3$  and  $\tau_4$  can be attributed to *o*-Ps annihilation in some small and large microvoids, respectively, and the *p*-Ps annihilation also adds its contribution to the first lifetime  $\tau_1$ .

After annealing at 800 °C, the first lifetime ( $\tau_1$ ) of as-prepared MgO reduced to 208 ps with the intensity of 42 % and still higher to that of reported positron bulk lifetime (166 ps) in MgO [28]. It is observed that all the lifetime is reduced for Li<sup>+</sup>-doped MgO nanocrystallites annealed at 800 °C. Most significantly, first lifetime of Li-doped MgO is reduced to 161 ps. This explains clearly that Li<sup>+</sup> migrates to occupy Mg vacancy site and hence the intensity ( $I_1 = 65$  %) is increased, thereby increasing the electron density nearby. The ionic radius of Li<sup>+</sup> is 0.68 Å and Mg<sup>2+</sup> is 0.65 Å; hence, the same radii have been balanced with the charges (two Li ion balanced with one oxygen). The other three component intensities ( $I_2$ ,  $I_3$ , and  $I_4$ ) are reduced owing to doped Li ion which reduces the cluster vacancies

**Fig. 1** Positron lifetime and relative intensity of as-prepared and doped MgO



and microvoids. We can conclude that the vacancy defects in the crystallites and grain boundary region are reduced for Li-doped MgO, whereas prompt recovery of Mg vacancy is observed after annealing at 800 °C.

Na<sup>+</sup>- and K<sup>+</sup>-doped MgO shows the same behavior for the first lifetime, and this ion tends to move to the substitutional positions, thereby slightly reducing the first lifetime values and their intensity since Na<sup>+</sup> (0.97 Å) and K<sup>+</sup> (1.33 Å) have bigger ionic radii compared to Mg<sup>2+</sup>. This lifetime is around 195 ps which is still more than the positron bulk lifetime in MgO. It is suggested that only minor fraction of the ions tends to move into Mg

substitutional positions and the remaining reside on the surface or on the grain boundaries of nanocrystallites to yield optimum strain relief [32]. This indicates that some residual vacancies still remain after annealing. The intensity  $I_1$  is reduced to 33 and 36 % for Na and K doping which indicates vacancies agglomerate to cluster vacancies, thereby increasing the intensity  $I_2$  and  $I_3$ . These might be due to some of the vacancies agglomerated as cluster vacancy and some cluster vacancies agglomerated as small microvoids. Still the  $\tau_4$  component is almost same because the large pores have high thermal stability and the corresponding large pores are most probably the unoccupied

**Table 1** Crystallite size and analyzed PAL spectral data for as-prepared and annealed MgO samples

Sample	MgO		MgO:Li		MgO:Na		MgO:K	
Temperature (°C)	500	800	500	800	500	800	500	800
Crystallite size (nm)	22	32	21	34	28	36	19	35
$\tau_{av}$ (ns)	0.6755	0.7552	0.5530	0.3654	0.4123	0.4268	0.4028	0.4032
Pore radius	2.96	2.66	2.92	2.54	2.51	2.28	2.29	2.17
$R_1$ (Å)								
Pore radius	8.9	9.44	9.03	7.82	6.86	7.2	7.05	7.09
$R_2$ (Å)								

space between inter connected nanograins [33]. Wang et al. [34] also reported such large pores through positronium formation in ZnO nanocrystals. In the present study, these large pores are not disappeared even after annealing at 800 °C and indicate that the densification of MgO nanocrystals is more difficult than ZnO [30].

These *ortho*-positronium components undergo 2-gamma pick-off annihilation when the positron localized in voids and their lifetime are few tens of ns that depend on the void size which are observed here as  $\tau_3$  and  $\tau_4$  components. The intensity of this lifetime reflects the relative number of the pores. The annihilation lifetime contains information about the pore size which can be extracted by calculating the annihilation rate of *o*-Ps as,

$$\frac{1}{\tau_{o-Ps}} = \lambda_{o-Ps} = \lambda_{2\gamma} + \lambda_{3\gamma} = \lambda_{2\gamma}^0(P) + \lambda_{3\gamma}^0(1 - P) \quad (1)$$

where  $P$  is the probability to find *o*-Ps in the wall of the pore. Several models have been proposed for obtaining a correlation between the positron lifetime and the sizes of micropores with various shapes for porous materials. The correlation of the lifetime to a pore size is often carried out via the semiempirical quantum mechanical model of Tao and Eldrup [35, 36]. The expression conducting *o*-Ps pick-off lifetime and free volume radius,  $R$ , according to Tao [35], Eldrup et al. [36], and Nakanishi et al. [37]

$$\lambda_{TE}(R) = \lambda_A \left[ 1 - \frac{R}{R + \Delta R} + \frac{1}{2\pi} \sin\left(\frac{2\pi R}{R + \Delta R}\right) \right] \quad (2)$$

where  $\lambda_A = (\lambda_S + 3\lambda_T)/4$  is the spin-averaged vacuum annihilation rate and  $\lambda_S$  and  $\lambda_T$  are the singlet and triplet vacuum annihilation rates.  $R_0 = R + \Delta R$  where  $\Delta R$  is the fitted empirical electron layer thickness ( $=1.66 \text{ \AA}$ ). The lifetime is  $\tau = \frac{1}{\lambda}$ . From *o*-Ps lifetime, the mean free volume pore radius ( $R$ ) can be obtained.

$$\tau_{o-Ps} = \frac{1}{2} \left[ 1 - \frac{R}{R_0} + \frac{1}{2\pi} \sin\left(\frac{2\pi R}{R_0}\right) \right]^{-1} \quad (3)$$

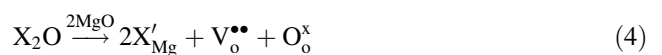
where  $\tau_{o-Ps}$  (*o*-Ps lifetime) and  $R$  (Pore radius) are expressed in ns and Å, respectively. The spherical pore radius was estimated in Table 1. Both pore radii  $R_1$  and  $R_2$  for Li-doped MgO decrease as well as vacancy and cluster

vacancy for sample annealed at 800 °C. This reveals that most of the Li ion occupied by vacancies and voids. On the contrary,  $R_2$  slightly increased for Na- and K-doped MgO and is due to some of the small pores agglomerated to increase the big void structure.

### 3.2 Doppler broadening studies

From the DB studies, the resultant changes in the spectra are characterized for the  $S$  parameter, which mainly reflects changes due to the annihilation of positron–electron pairs with a low-momentum distribution, and by the  $W$  parameter, which mainly characterizes changes due to the annihilation of pairs with a high-momentum distribution. In general, the characteristic value of  $S$  ( $W$ ) expected for the annihilation of positrons due to their trapping by vacancy-type defects is larger (smaller) than that for positrons annihilated from the free state. Figure 2 represents the clear interpretation of the coincidence Doppler broadening  $S$  versus  $W$  parameters. Li-doped MgO shows decrease in  $S$  parameter after annealing to 800 °C. This represents the major recovery of vacancy defects or reduction in defect concentrations. Na and K ions which were on the surface tend to move into the MgO lattice after annealing at 800 °C; thus, after annealing, the free volume size increases owing to the growth on the boundary line, thereby increasing its crystallite size and hence decreases the electron density. The ionic radii of  $\text{Na}^+$  and  $\text{K}^+$  are slightly bigger than that of the  $\text{Mg}^{2+}$ , and this bigger ions tend to occupy substitutional positions and on the surface regions. Thus, the  $S$  parameter gets increased for Na and K dopants at 800 °C. From this CDB measurement, the positron trapping sites were identified as vacancy clusters.

The vacancies were created by replacing  $\text{Mg}^{2+}$  by alkali metal ions as given by Eq. (4) [23]



the  $\text{X}^+$  ions (alkali metal ion) replacing  $\text{Mg}^{2+}$  ion are considered as negative lattice defects ( $\text{X}'_{\text{Mg}}$ ), oxygen vacancies  $\text{V}_\text{o}^{\bullet\bullet}$  as positive defects (2 positive charges), and  $\text{O}_\text{o}^x$  is normal or regular occupied oxygen or anion sites. The charges of one oxygen vacancy are compensated by the charges of two

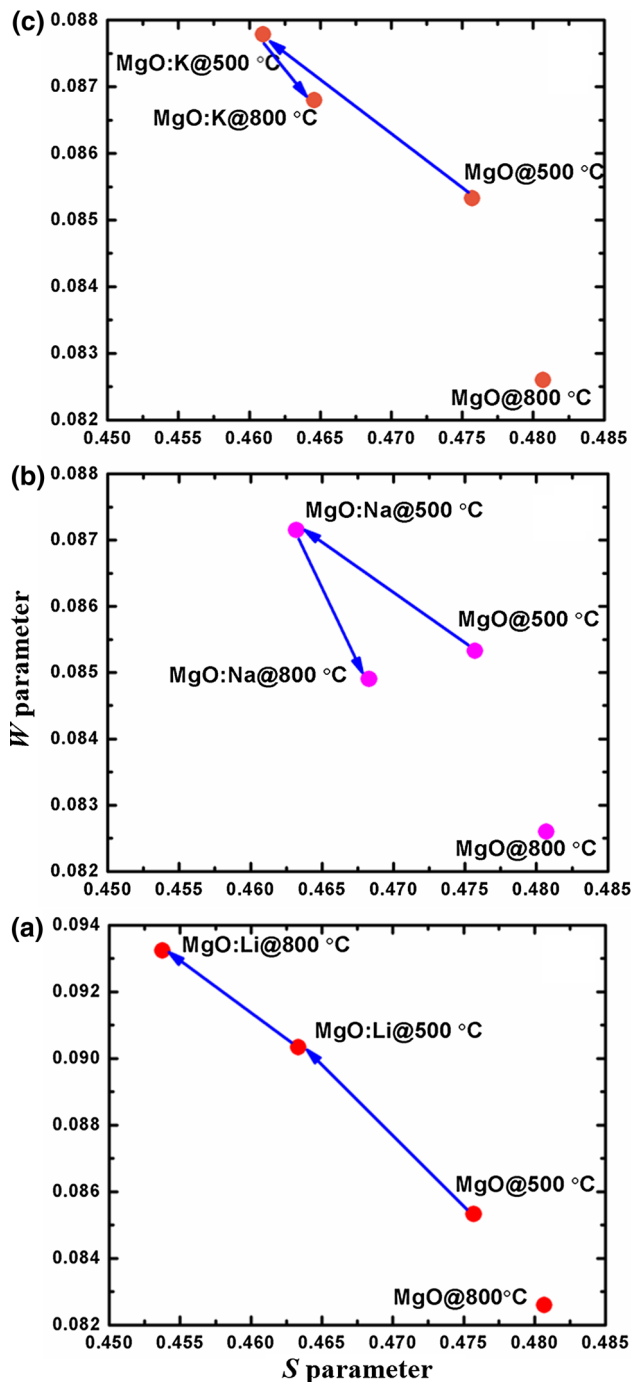


**Fig. 2**  $S$ – $W$  parameter of as-prepared (500 °C) and 800 °C annealed MgO. **a** MgO:Li, **b** MgO:Na, and **c** MgO:K (The arrows are only to show the trend)

$X^+$  ions, which will lead to MgO lattice distortion, causing stress [38]. Impurities can carry a charge relative to the host structure with a Li ion substituted on a Mg site in MgO. As the impurity carriers have a different chemical valence than the host atoms, the introduction of charged impurities will upset the charge neutrality of the Mg. To balance the

electronic neutrality, the ionic/structural compensation can be achieved by the incorporation of other Li interstitial atoms that carry a balancing charge. Even the Na and K balancing the charge, the big ionic radii when compared to the Mg are given the stress and it is migrated in the substitutional positions and on the grain boundaries region. Hence, the  $S$  parameter slightly increased at that particular temperature when compare to 500 °C.

### 3.3 Average lifetime versus $S$ parameter

The average positron lifetime is calculated using the formula mentioned in Eq. (5).

$$\tau_{av} = \frac{\sum \tau_i I_i}{\sum I_i} \quad (5)$$

where  $\tau_i$  is the positron lifetime and its corresponding  $I_i$  ( $i = 1, 2, 3$  and 4) [39]. Figure 3 shows comparison of the average positron lifetime and  $S$  parameter which are given that of complimentary information for all samples.  $S$  parameter shows reduction in defects, which is same from the lifetime result.  $S$  parameter contains the information of not only the short lifetime components, but also the positronium annihilation [30].

Average lifetime of as-prepared MgO annealed at 800 °C shows clearly the vacancy and vacancy clusters are agglomerated which increase the average lifetime and  $S$  parameter at the particular temperature as shown in Fig. 3. But the doped MgO at 800 °C shows clearly that Li, Na, and K ion occupied in the vacancy, cluster vacancy, and open pores. The averaged lifetime and  $S$  parameter of Na- and K-doped samples are almost similar for 800 °C sample compared with 500 °C annealed samples. The slight variation in both values is Na and K ions tend to move from grain boundary to the intercrystallite regions. The average lifetime reflects the overall information about the vacancy defects. Doping reduces the Mg vacancy after annealing to 800 °C. For 800 °C annealed MgO, the  $\tau_{av}$  (0.7552 ns) represents the number of vacancies, cluster vacancies and open pores (microvoids). The decrease in  $\tau_{av}$  (0.3654, 0.4268, and 0.4032 ns) for MgO:Li, MgO:Na, and MgO:K with respect to pure MgO shows that alkali metal ions get substituted in Mg sites in MgO lattice. In the present work, the observation that the average lifetime and  $S$  parameter decreases with increase in particle size as shown in Table 1, which suggests that the concentration of surface defect decreases with increasing particle size (~22 to 35 nm). Even though the fraction of positrons diffused to the grain boundary region is reduced with increasing grain size [30], Li-doped MgO has completely reduced Mg vacancy-type defect and existing cluster vacancy and micropores. In all other samples, the aforementioned defects still exist.

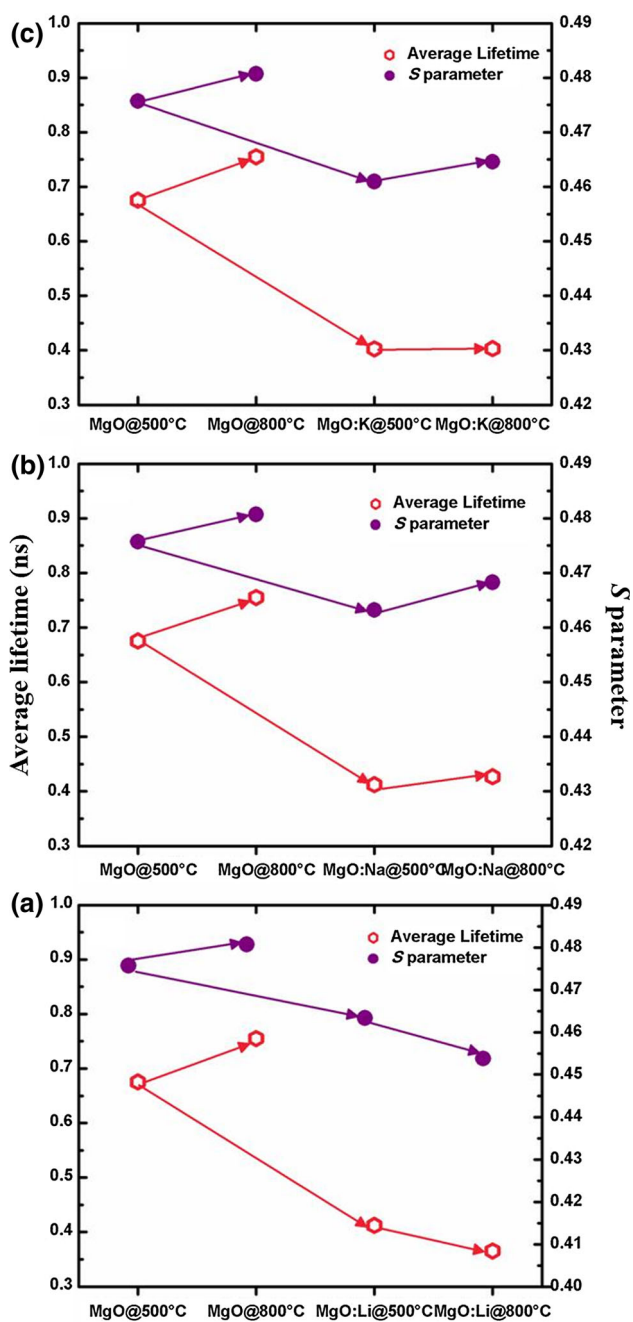


**Fig. 3** Average lifetime versus  $S$  parameter of as-prepared (500 °C) and 800 °C annealed MgO. **a** MgO:Li, **b** MgO:Na, and **c** MgO:K (The arrows are only to show the trend)

### 3.4 Photoluminescence (PL) studies

Photoluminescence emission spectra of as-prepared and 800 °C annealed MgO and alkali metal ion-doped MgO were recorded at the excitation wavelength of 370 nm in the range of 375–700 nm (Fig. 4a–d). Earlier reports remarked that the emission peaks from MgO are not due to the band gap and attributed to the various native structural defects

formed between the band gap [40]. Defects such as oxygen vacancies, F centers (oxygen ion vacancies occupied by two electrons),  $F^+$  centers (oxygen ion vacancies occupied by single electrons),  $F^{2+}$  (oxygen vacancy without any electron), and surface states are responsible for the photoluminescence properties of MgO [41]. The PL spectra of as-prepared and 800 °C annealed MgO consist of two peaks at 445 and 498 nm which are attributed to the structural defects. The emission peak at 445 nm is associated with  $F_2^{2+}$ , and the emission peak 498 nm is assigned to recombination of higher-order vacancy complexes [42]. On annealing alkali-doped MgO at 800 °C, a small sharp peak emerges at 416 nm which is attributed to F center [41].

Lu et al. [43] and Wu et al. [44] reported the substitution of  $Na^+$  ion in  $Zn^{2+}$  site of ZnO, and the oxygen created from charge compensation is well proved from PL analysis. In K-doped ZnO, substitution of  $K^+$  ion in  $Zn^{2+}$  site of ZnO is examined through PL spectra [45, 46]. Similarly, oxygen vacancies created by substitution of  $Ni^+$  ion in  $Zn^{2+}$  site was also observed by Iqbal et al. [47]. In our earlier work, the substitution of alkali in  $Mg^{2+}$  site is well showed in XRD analysis [25]. Here, we have already proved the substitution of alkali ion ( $Li^+$ ,  $Na^+$  and  $K^+$ ) in Mg site through positron annihilation studies. Now, an attempt is made to prove the substitution of alkali ion in  $Mg^{2+}$  site of MgO lattice through PL spectra. It is well known that charge compensation between  $Mg^{2+}$  and dopant creates anion vacancies in MgO lattice. It is supposed to be an anion vacancy charge-compensated by two  $X^+$  ( $X = Li, Na, \text{ and } K$ ) ions, with the linear configuration:  $O^{2-}-X^+-[oxygen\ vacancy]-X^+-O^{2-}$  [48]. Alkali dopant in MgO appears as defect complexes, comprising alkali dopant and O defects, and therefore neutralizes the effect of the alkali dopant [32]. On annealing the alkali-doped MgO at 800 °C, the emission peak due to oxygen vacancy increases sharply. In addition to that, thermal annealing process (800 °C) is likely to dissociate  $F_2^{2+}$  to  $F^+$ , and finally, this  $F^+$  is converted into F centers. Therefore, an emission corresponds to F center appears in alkali-doped MgO annealed sample. Thus, from the PL study, it is concluded that optical property of MgO has been enhanced due to the oxygen vacancies by substitution of alkali ion in Mg site.

### 4 Conclusion

Positron annihilation measurements reveals the vacancy defects such as Mg vacancies, vacancy clusters, and microvoids in the crystallite and grain boundary region. It confirms the presence of Mg vacancies in the crystal lattice and grain boundary, and the concentration of Mg vacancies is reduced after doping with alkali metal ions. Thus, alkali

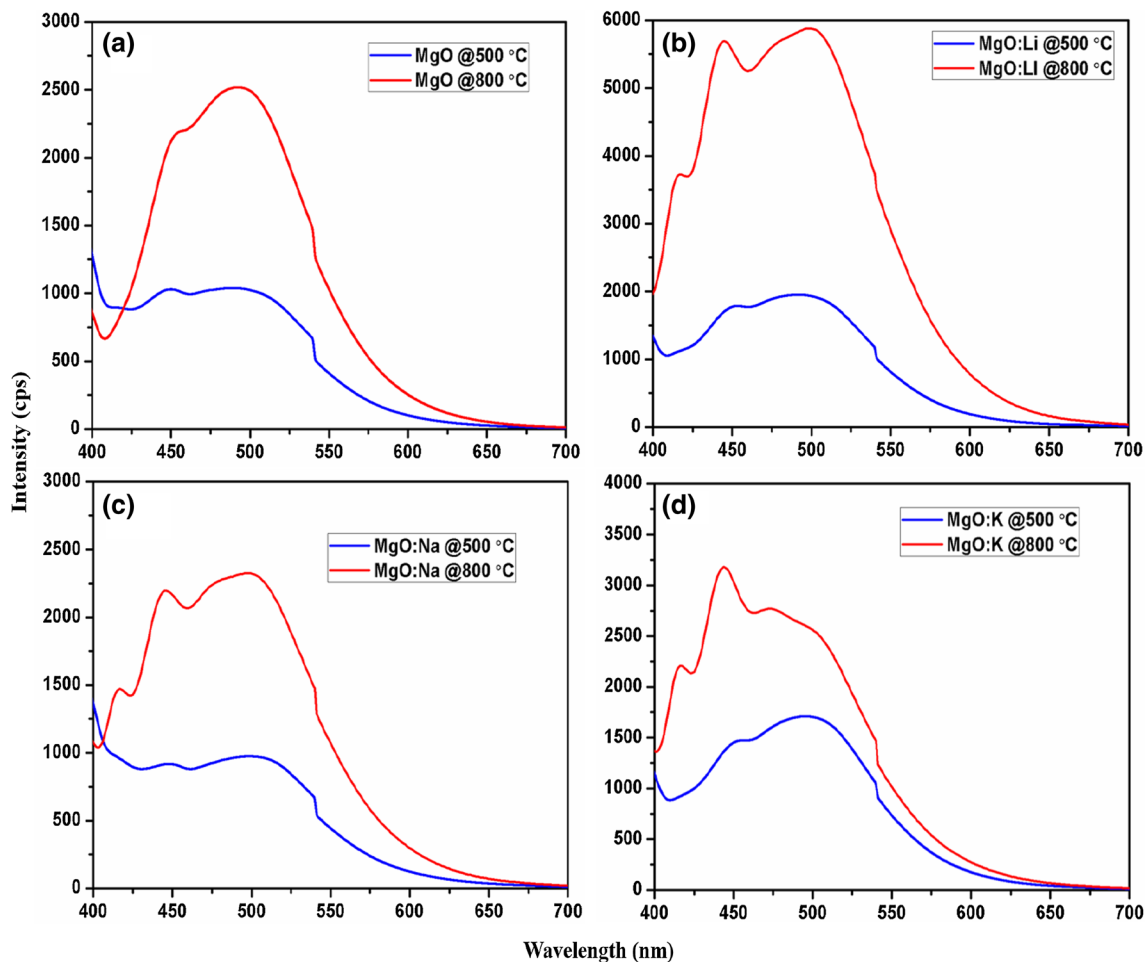


**Fig. 4** Photoluminescence spectra of as-prepared (500 °C) and 800 °C annealed. **a** Pure MgO, **b** MgO:Li, **c** MgO:Na, and **d** MgO:K

metal ions are occupied in the Mg-related vacancies, thereby increasing the crystallite size at 800 °C. Rapid recovery of Mg vacancies is observed for Li-doped sample after annealing at 800 °C. The variation in vacancy defects in Na- and K-doped MgO nanocrystals during annealing is reflected by the two shorter lifetime components. Average lifetime and the  $S$  parameter of doped MgO at 800 °C clearly shows that, Li, Na, and K ions are occupied in the vacancy and cluster vacancies and are due to particle growth and reduction in the defect concentration. From the PL study, the emission peak at 445 nm and 498 nm is associated with  $F_2^{2+}$  and recombination of higher-order vacancy complexes, respectively. An anion vacancy has been charge-compensated by two  $X^+$  ( $X = \text{Li, Na, and K}$ ) ions, with the linear configuration:  $\text{O}^{2-}-\text{X}^+[\text{oxygen vacancy}]-\text{X}^+-\text{O}^{2-}$ . Thermal annealing process (800 °C) is likely to dissociate  $F_2^{2+}$  to  $F^+$ , and finally, this  $F^+$  is converted into F centers emerges at 416 nm.

**Acknowledgments** The authors are thankful to Dr. Shanmugavel Chinnathambi, for PL measurement at the National Institute for Materials Science (NIMS), Japan.

## References

1. A.L. Linsebigler, G.Q. Lu, J.T. Yates Jr., *Chem. Rev.* **95**, 735 (1995)
2. M.R. Hoffmann, S.T. Martin, W.Y. Choi, D.W. Bahnemann, *Chem. Rev.* **95**, 69 (1995)
3. J. Bisquert, D. Cahen, G. Hodes, S. Ruhle, A. Zaban, *J. Phys. Chem. B* **108**, 8106 (2004)
4. D.F. Watson, G.J. Meyer, *Annu. Rev. Phys. Chem.* **56**, 119 (2005)
5. S. Shukla, R. Agrawal, H.J. Cho, S. Seal, L. Ludwig, C.J. Parish, *Appl. Phys.* **97**, 054307 (2005)
6. A. Subramania, G.V. Kumar, A.S. Priya, T. Vasudevan, *Nanotechnology* **18**(22), 225601 (2007)
7. J.Y. Kim, H.S. Jung, K.S. Hong, *J. Am. Ceram. Soc.* **88**(3), 784–787 (2005)
8. M.S. El-Shall, W. Slack, W. Vann, D. Kane, D. Hanley, *J. Phys. Chem.* **98**(12), 3067–3070 (1994)
9. Y. Ding, G. Zhang, H. Wu, B. Hai, L. Wang, Y. Qian, *Chem. Mater.* **13**(2), 435–440 (2001)
10. K.P. McKenna, D. Koller, A. Sternig, N. Siedl, N. Govind, P.V. Sushko, O. Diwald, *ACS Nano* **5**(4), 3003–3009 (2011)
11. T. Makino, K. Tamura, C.H. Chia, Y. Segawa, M. Kawasaki, A. Ohtomo, H. Koinuma, *Phys. Rev. B* **65**, 121201–121204 (2002)
12. R.J.D. Tilley, *Defects in Solids* (Wiley, New Jersey, 2008)



13. E. Scorza, U. Birkenheuer, C. Pisani, J. Chem. Phys. **107**(22), 9645–9658 (1997)
14. K. Mageshwari, S.S. Mali, R. Sathyamoorthy, P.S. Patil, Powder Technol. **249**, 456–462 (2013)
15. S. Stankic, M. Sterrer, J. Bernardi, O. Diwald, E. Knözinger, Nano Lett. **5**, 1889 (2005)
16. B.L. Abrams, P.H. Holloway, Chem. Rev. **104**, 5783 (2005)
17. P.B. Devaraja, D.N. Avadhani, H. Nagabhushana, S.C. Prashantha, S.C. Sharma, B.M. Nagabhushana, H.P. Nagaswarupa, B.D. Prasad, J. Radiat. Res. Appl. Sci. **8**(3), 362–373 (2015)
18. P. Rinke, A. Schleife, E. Kioupakis, A. Janotti, C. Rödl, F. Bechstedt, M. Scheffler, C.G. Van de Walle, Phys. Rev. Lett. **108**, 126404 (2012)
19. P.V. Pikhitsa, C. Kim, S. Chae, S. Shin, S. Jung, M. Kitaura, S.I. Kimura, K. Fukui, M. Choi, Appl. Phys. Lett. **106**, 183106 (2015)
20. J. Xu, A.P. Mills Jr., A. Ueda, D.O. Henderson, R. Suzuki, S. Ishibashi, Phys. Rev. Lett. **83**(22), 4586–4589 (1999)
21. M.C. Wu, C.M. Truong, D.W. Goodman, Phys. Rev. B **46**, 12688 (1992)
22. X. Lu, X. Xu, N. Wang, Q. Zhang, J. Phys. Chem. B **103**, 3373 (1999)
23. I. Balint, K. Aika, Appl. Surf. Sci. **173**, 296–306 (2001)
24. O. Runevall, N. Sandberg, Comput. Mater. Sci. **60**, 53–58 (2012)
25. J. Sivasankari, S. Selvakumar, K. Sivaji, S. Sankar, J. Alloys Compd. **616**, 51–57 (2014)
26. H. Saito, T. Hyodo, Radiat. Phys. Chem. **68**, 431 (2003)
27. M.A. Monge, R. Pareja, R. Gonzalez, Y. Chen, Phys. Rev. B **55**, 243 (1997)
28. N.H. Hong, J. Sakai, N. Poirot, V. Brizé, Phys. Rev. B **73**, 132404 (2006)
29. T.E.M. Staab, R. Krause-Rehberg, B. Kieback, J. Mater. Sci. **34**(16), 3833–3851 (1999)
30. D.D. Wang, Z.Q. Chen, C.Y. Li, X.F. Li, C.Y. Cao, Z. Tang, Phys. B **407**, 2665–2669 (2012)
31. M. Chandrasekhar, H. Nagabhushana, S.C. Sharma, K.H. Sudheerkumar, N. Dhananjaya, D.V. Sunitha, C. Shivakumara, B.M. Nagabhushana, J. Alloys Compd. **584**(25), 417–424 (2014)
32. N.A. Richter, F. Stavale, S.V. Levchenko, N. Nilius, H.-J. Freund, M. Scheffler, Phys. Rev. B Condens. Matter **91**, 195305 (2015)
33. A. Karbowski, K. Fedus, J. Patyk, L. Bujak, K. Służewski, G. Karwasz, Nukleonika **58**, 189–194 (2013)
34. D. Wang, Z.Q. Chen, D.D. Wang, N. Qi, J. Gong, C.Y. Cao, Z. Tang, J. Appl. Phys. **107**, 023524 (2010)
35. S.J. Tao, J. Chem. Phys. **56**, 5499–5510 (1972)
36. M. Eldrup, D. Lightbody, J.N. Sherwood, Chem. Phys. **63**, 51–58 (1981)
37. H. Nakanishi, S.J. Wang, Y.C. Jean, in *Positron Annihilation Studies of Fluids*, ed. by S.C. Sharma (World Scientific, Singapore, 1988), p. 292
38. L. Xu, F. Gu, J. Su, Y. Chen, X. Li, X. Wang, J. Alloys Compd. **509**, 2942–2947 (2011)
39. Y.-H. Lin, M. Li, C.-W. Nan, Z. Zhang, J. Am. Ceram. Soc. **90**, 2991–2994 (2007)
40. Q. Wang, N. Holzwarth, Phys. Rev. B Condens. Matter **41**, 3211 (1990)
41. B. Choudhury, P. Basyach, A. Choudhury, J. Lumin. **149**, 280–286 (2014)
42. M.L. Bailly, G. Costentin, H. Lauron-Pernot, J.M. Krafft, M. Che, J. Phys. Chem. B **109**, 2404 (2005)
43. J. Lü, K. Huang, J. Zhu, X. Chen, X. Song, Z. Sun, Phys. B Matter **405**(15), 3167–3171 (2010)
44. C. Wu, Q. Huang, J. Lumin. **130**(11), 2136–2141 (2010)
45. L. Xu, X. Li, J. Yuan, Superlattices Microstruct. **44**(3), 276–281 (2008)
46. M.K. Gupta, N. Sinha, B.K. Singh, B. Kumar, Mater. Lett. **64**(16), 1825–1828 (2010)
47. J. Iqbal, B. Wang, X. Liu, D. Yu, B. He, R. Yu, New J. Phys. **11**(6), 063009 (2009)
48. R. González, Y. Chen, Phys. Rev. B Condens. Matter **35**(15), 8202 (1987)